Resources, Conservation & Recycling 178 (2022) 106050

Contents lists available at ScienceDirect

Resources, Conservation & Recycling

journal homepage: www.elsevier.com/locate/resconrec

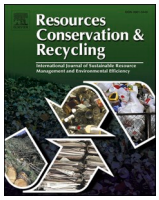

A thermodynamics-guided framework to design lightweight aggregate from waste coal combustion fly ash

Mohammad Balapour [a,*], Thiha Thway [b], Rathin Rao [c], Newell Moser [d], Edward J. Garboczi [d], Y Grace Hsuan [a], Yaghoob Farnam [a]

[a] Drexel University, Department of Civil, Architectural and Environmental Engineering, 3141 Chestnut Street, Philadelphia, PA 19104, United States
[b] Drexel University, Department of Chemical Engineering, 3141 Chestnut Street, Philadelphia, PA 19104, United States
[c] Drexel University, Department of Mechanical Engineering and Mechanics, 3141 Chestnut Street, Philadelphia, PA 19104, United States
[d] National Institute of Standards and Technology, Applied Chemicals and Materials Division, Boulder, CO 80305, United States

ARTICLE INFO

Keywords:
Off-spec fly ash
Liquid phase
Viscosity
Gas release
Thermodynamics modeling

ABSTRACT

A systematic thermodynamics-based framework was applied to recycle waste low and high-calcium coal combustion Fly Ash (FA) into synthetic lightweight aggregates (LWA) through sintering. The process to successfully manufacture synthetic LWA was investigated, which requires a delicate balance among three phenomena: (i) sufficient liquid phase formation during sintering, (ii) appropriate viscosity for the liquid-solid phase, and (iii) sufficient amount of gas emission to form pores in the LWA. Thermodynamics modeling was used to quantify the formation of the liquid phase during sintering while the fluxing agent and the temperature change. The Urbain-Kalmanovitch, Browning, and Krieger-Dougherty models were used to quantify the viscosity of the liquid and liquid-solid phase, respectively. A lower bound of 100 Pa•s for the viscosity was found to ensure spherical shape of the LWA. Using thermogravimetric analysis, it was shown that the LWA had a notable gas release potential, owing to the presence of anhydrite and hematite, which could create gas-filled pores in the LWA macro-microstructure. X-ray computed tomography (X-CT) observation revealed the formation of a porous structure for the produced LWA where high calcium FA LWA generally had larger pores compared with low calcium FA LWA. By correlating the X-CT and scanning electron microscopy (SEM) observations and thermodynamic modeling results, it was found that a minimum of 40% liquid phase content (% by mass) is necessary for the formation of gas-filled pores in FA-LWA.

1. Introduction

Lightweight aggregates (LWA) as a construction material has a wide range of applications including lightweight concrete production, internal curing of concrete, green roofs, and embankment. At present, most of the available lightweight aggregates (LWA) in the US market are expanded shale, clay, and slate-based, which are only available in North Carolina, up-state New York, Texas, Kansas, Colorado, California, and Indiana. This fact has a direct impact on the accessibility and final price of LWA due to the cost of transportation (Mousa et al., 2018). Additionally, these LWAs require the use of natural resources (i.e., shale, clay, and slate) as their feed materials during manufacturing. In recent years, there have been many efforts to explore LWA production from urban and industrial wastes to not only increase LWA availability and accessibility in different regions, but also to address the growing concerns over sustainability (Dondi et al., 2016; Cheeseman et al., 2005).

Waste (i.e., not recycled) coal combustion products (CCPs) including fly ash (FA), bottom ash (BA), and boiler slag need to be landfilled (Kourti and Cheeseman, 2010; Balapour et al., 2020) if it they are not recycled. In 2018, over 100 million tonne of coal combustion ash were produced, of which about 60 million tonne were beneficially recycled and the rest disposed in landfills (Association, 2018). Over time, this gap in recycling has left the U.S. with a large stock of waste CCPs in landfills, which is negatively impacting the environment (e.g., polluting surface and groundwater) and human health (Billen et al., 2018; EPA, 2015). Rules issued by Environmental Protection Agency (U.S. EPA) on disposal of waste CCPs in 2015 (EPA, 2015) required closure or retrofit of unsafe landfills or surface impoundments, increasing the cost associated with disposal of waste CCPs, and therefore, increasing the recycling incentives for waste CCPs. Converting the waste CCPs available in the

* Corresponding author
E-mail address: mb3746@drexel.edu (M. Balapour).

https://doi.org/10.1016/j.resconrec.2021.106050
Received 27 May 2021; Received in revised form 13 October 2021; Accepted 9 November 2021
Available online 16 November 2021

Nomenclature

Andradite $Ca_3Fe_2Si_3O_{12}$
Anhydrite $CaSO_4$
Anorthite $CaAl_2Si_2O_8$
Clinopyroxene $CaMgSi_2O_6$
Combeite $Na_2Ca_2Si_3O_9$
Cordierite $Mg_2Al_4Si_5O_{18}$
Dolomite $CaMg(CO_3)_2$
Feldspar (Albite) $NaAlSi_3O_8$
Feldspar (Anorthite) $CaAl_2Si_2O_8$
Feldspar (K-Feldspar) $KAlSi_3O_8$
Gypsum $CaSO_4 \bullet 2H_2O$
Hematite Fe_2O_3
Leucite $KAlSi_2O_6$
Melilite $Ca_2Mg(Si_2O_7)$
Mullite $3Al_2O_3 \bullet 2SiO_2$
Nepheline $NaAlSiO_4$
Sapphirine $Mg_4Al_{10}Si_2O_{23}$
Tridymite SiO_2
Wollastonite $CaSiO_3$
C: CaO, A: Al_2O_3, N: Na_2O, S: SiO_2, H: H_2O C-A-(N)-S-H
N: Na_2O, A: Al_2O_3, S: SiO_2, H: H_2O N-A-S-H

landfills to LWA is a viable solution to both reduce landfilled waste CCPs and increase LWA accessibility for the construction industry (Dondi et al., 2016).

There have been several efforts to convert waste CCPs to LWA (Dondi et al., 2016; Balapour et al., 2020; Balapour et al., 2019; Wei and Lin, 2009; Wei et al., 2012; Ramamurthy and Harikrishnan, 2006; Kockal and Ozturan, 2010). In these, FA and BA have been reported as suitable raw materials for producing synthetic LWA. It has been shown that sintering class F (low calcium) fly ash mixed with 0% to 30% (by mass) sodium bentonite as a binder at 1100 °C for 1 h could result in an LWA with specific gravity of 1.75 to 2 and a corresponding 24 h water absorption of 21% and 16%, respectively (Ramamurthy and Harikrishnan, 2006). In another study, class F fly ash LWA with 0% and 5% glass powder (added as a fluxing agent) was manufactured (Kockal and Ozturan, 2010). For LWA without glass powder (main chemical oxides were SiO_2, CaO, and Na_2O), oven-dry specific gravity, water absorption, and crushing strength were determined to be 1.51, 18.4%, and 5.1 MPa, respectively. While, the addition of 5% glass powder as fluxing agent increased the specific gravity to 1.81 and led to a stronger LWA with a crushing strength of 9.7 MPa.

Previous studies suggest (Dondi et al., 2016; Verbinnen et al., 2017; Riley, 1951; Balapour et al., 2021) that LWA production through a sintering process requires three necessary conditions: (i) formation of a sufficient amount of liquid phase at high temperature on the surface of the aggregate to maintain a viscous state, (ii) appropriate viscosity for the liquid-solid phase to ensure pore expansion while preventing excessive deformation, and (iii) appropriate amount of gas release, close to the sintering temperature, which can be entrapped by the liquid phase, leading to expansion and LWA formation. Bloating mechanism is defined as the co-occurrence of these three conditions during sintering resulting in formation of a successful LWA with a porous macro-microstructure (Dondi et al., 2016; Balapour et al., 2019; Aineto et al., 2006). Providing an appropriate balance among these three conditions can lead to tailored, superior LWA engineering properties, such as specific gravity, compressive strength, and moisture dynamics.

Balapour et al. (Balapour et al., 2021) proposed a thermodynamics-based approach to quantify each of the three aforementioned conditions for LWA produced from high- and low-calcium BA, where NaOH was used as a fluxing agent. Based on these three conditions, they proposed a working zone (i.e., quantitative limits for liquid phase content, viscosity value, and amount of gas release) that can ensure successful LWA production. The authors manufactured spherical BA-LWA, where the spherical shape of LWA was intended to increase concrete workability when used for concrete production. Their approach demonstrated that when produced with this method BA-LWA possessed an oven-dry specific gravity of 0.9 to 1.3, a porosity of 40% to 60%, and a 72 h water absorption of 15% to 45%. These superior engineering properties were related to the controlled formation of a porous microstructure during the sintering. The potential performance of these LWA for internal curing of concrete was also found to be promising (Balapour et al., 2020; Balapour, 2020).

The work presented in this paper builds on previous work (Balapour et al., 2020; Billen et al., 2018; Balapour et al., 2019; Balapour et al., 2021) and establishes a predictive thermodynamics-based framework to quantitatively address the three necessary conditions for successful production of LWA from **waste coal combustion fly ash (FA)** through a sintering process. In this study, thermodynamics modeling was first performed to quantify the liquid phase formation in the system of FA and NaOH (used as a fluxing agent). Second, using these thermodynamics modeling results, the viscosity of the LWA liquid-solid phase formed

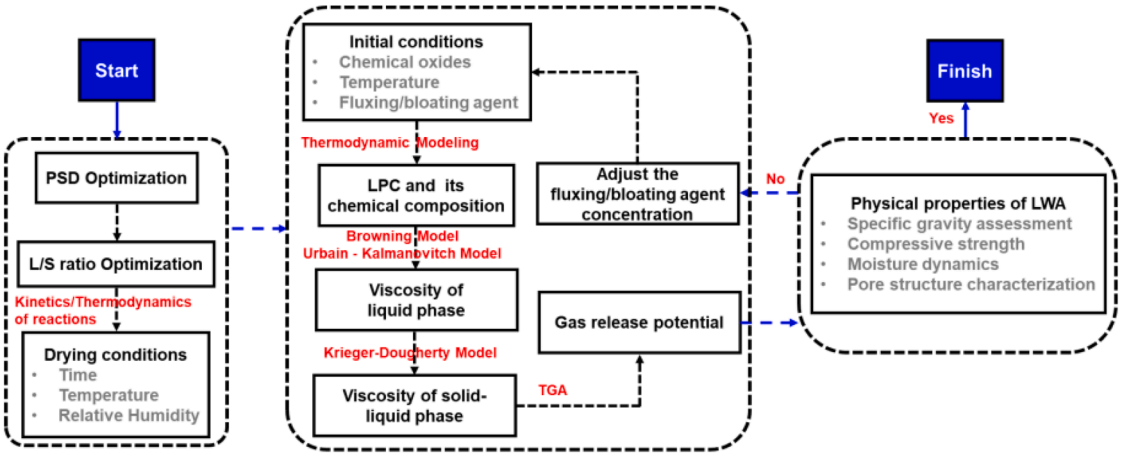

Fig. 1. Extended thermodynamics-based framework for production of LWA independent of feed materials.

during the sintering was estimated by employing a combination of the Urbain- Kalmanovitch, Browning and Krieger-Dougherty (K-D) models. Third, the gas release potential of the LWA necessary for pore formation was quantified using thermogravimetric analysis (TGA). Finally, using X-ray computed tomography (X-CT) and scanning electron microscopy (SEM), the pore structure of the developed LWA was visualized and evaluated. The technological adoption of the thermodynamics-based framework presented in this study will pave the way to consider waste CCPs as a highly suitable resource to produce value-added LWA for concrete applications.

2. Extended thermodynamics-guided framework for LWA production

Fig. 1 outlines the extended thermodynamics-guided framework for LWA production, independent of feed materials. The figure considers three major steps for successful LWA production. The first step is the production of spherical fresh pellets from the feed materials. This procedure starts with particle size distribution (PSD) optimization of the feed materials as this physical property can affect the engineering properties of the final LWA product (Dondi et al., 2016; Balapour et al., 2020). Afterward, an optimum liquid to solid ratio should be determined to achieve desired workability, binding, and cohesiveness for formation of the fresh spherical pellets. Note that the liquid here is a mixture of water and a fluxing agent at a specific concentration. The first step ends by drying the fresh pellets in a controlled temperature/humidity condition for a given duration prior to the sintering.

The second step, which is the focus of this paper, is associated with the optimization of the sintering process to produce LWA. This step starts by inputting the chemical composition of the raw material, the temperature of interest, and the dosage of fluxing or bloating agents into a thermodynamics model. The predictions of the thermodynamics modeling include the formation of different phases and, more importantly, the amount of liquid phase and its chemical composition that will be formed within the targeted sintering temperature range. The liquid phase quantity and its chemical composition are then analyzed using the Urbain- Kalmanovitch (for low calcium fly ash) Browning model (for high calcium fly ash) to estimate the viscosity of the liquid phase during the sintering. Subsequently, the estimated viscosity of the liquid phase and quantity of solid phase are input into the K-D viscosity model (detailed discussion is provided in Section 0) to estimate the viscosity of the liquid-solid phase. TGA is then performed on the fresh pellets to quantify the gas release potential of materials, which is essential for the production of porous LWA.

In the third and final step, the physical and mechanical properties of the LWA, including specific gravity, compressive strength, moisture dynamics, and pore structure, are assessed. If those physical properties fall within the desired ranges, the LWA design will be finalized. Otherwise, the fluxing or bloating agent can be modified in the second step (as can be seen in Fig. 1) to go through the loop again to ensure that appropriate LWA physical properties are achieved.

Table 1
Chemical oxides of off-spec fly ash.

Chemical composition(% by mass)	Sample name	
	F-FA	C-FA
SiO_2	49.5	38.19
Al_2O_3	23.8	18.76
Fe_2O_3	15.45	10.88
SO_3	0.75	3.59
CaO	3.2	18.8
Na_2O	0.42	1.12
MgO	1.6	3.6
K_2O	2.3	0.98
P_2O_5	–	0.7
TiO_2	–	1.31
Total	97.02	97.93
LOI*	5.3	8.47
Unburnt Carbon	2.33	7.0
Initial moisture content	0.4	1.21

*The LOI is measured as the weight loss percentage between 110 °C and 750 °C.

Table 2
The crystalline phases content of raw fly ashes (percent by mass).

Phase name	Sample name	
	F-FA	C-FA
Quartz	7.03	5.93
Mullite	10.7	3.52
Hematite	4.49	1.04
Anhydrite	1.86	3
Calcium alumioferrite	0	1.57
Amorphous	75.9	84.9

3. Materials and sample preparation

Two types of waste coal combustion FA samples were used in this study using classifications defined in ASTM C618 (ASTM C618-19 2019): (i) class F (low calcium) fly ash, designated by F-FA; and class C (high calcium) fly ash, designated by C-FA. Table 1 shows the chemical oxide composition of the FA samples obtained through X-ray fluorescence (XRF). Waste coal combustion FA refers to the waste fly ash that does not pass at least one of the requirements proposed by ASTM C618 or AASHTO M 295 (AASHTO M 295 2007), and so cannot be directly used in concrete. One of the most important requirements of ASTM C618 for fly ash is that the Loss-on-Ignition (LOI) must be less than 6% by mass. In addition, based on AASHTO M 295, the LOI limit for fly ash, specified for use in concrete applications, must be less than 5% by mass in the majority of US states. Accordingly, fly ashes used in this study can be classified as waste coal combustion fly ash owing to a high LOI value (see *Table 1*).

Quantitative X-ray diffraction (QXRD) analysis was performed using nominally 0.02° steps in the range of 5° to 80° on the fly ashes (F-FA and C-FA) to quantify their amorphous content and crystalline phases. Rutile (TiO_2), nominally 20% by mass, was used as an internal standard for quantification. Table 2 shows the crystalline phases and amorphous content of the ashes, which indicates that a great portion of the ashes is composed of an amorphous phase.

The manufacturing of FA-LWA includes four main steps: drying, pelletization, curing, and sintering. In the first step, the ashes were dried in an oven at 110 °C ± 5 °C for approximately 24 h to remove moisture content. In the second step, dried ash was mixed with NaOH aqueous solution with molarities of 0 mol/L (i.e., pure deionized water), 2.5 mol/L, 5 mol/L, 7.5 mol/L, 10 mol/L, and 12.5 mol/L, with a liquid to solid mass (L/S) ratio of 0.2. These concentrations led to mass concentrations (i.e., mass of solid NaOH per mass of solid FA) of 0%, 2%, 4%, 6%, 8%, and 10%. The ash and aqueous NaOH (or deionized water) were mixed thoroughly to achieve a homogenous mixture, which was put into a spherical plastic mold of 16 mm diameter to pelletize the mixture. The L/S ratio of 0.2 mentioned earlier was found to be the minimum ratio that can maintain successful formation of spherical fresh pellets. In the third step, the pellet was cured in the environmental chamber at approximately 40 °C and 30% Relative Humidity (RH) for about 24 h. In the fourth and final step, the fresh aggregates were sintered at 1160 °C for 4 min to produce FA-LWA. Samples are designated as XXX-YY%, where XXX stands for the material type (F-FA or C-FA), while YY represents the NaOH concentration.

4. Research methodology

4.1. Analytical modeling

4.1.1. Thermodynamic modeling

Factsage[1] v7.2, a thermodynamic modeling software that operates based on Gibbs free energy minimization, coupled with its FT oxide database, was used to predict the phase equilibria of the ash+NaOH system for temperatures ranging from 800 °C to 1400 °C, in increments of 50 °C. The modeling was performed under 0.101 MPa (1 atm) pressure and ordinary air, which consisted of 0.21 mol fraction of oxygen and 0.79 mol fraction of nitrogen. The chemical oxides that were considered in the modeling and verified with XRF measurements included SiO_2, Al_2O_3, Fe_2O_3, SO_3, CaO, Na_2O, MgO, and K_2O.

4.1.2. Viscosity calculations

The viscosity of the liquid phase (slag) in LWA was quantified by employing two viscosity models. (i) The empirical viscosity model developed by (Browning et al., 2003) was used for estimating the viscosity of liquid phase in C-FA LWA. This empirical model has been shown to be more appropriate to calculate the viscosity of coal ash slag with a viscosity lower than 1000 Pa•s compared to other models that are based on simplified oxide melts (e.g. Urbain model) (Billen et al., 2018; Browning et al., 2003). (ii) For calculating the viscosity of liquid phase in F-FA LWA, widely used Urbain-Kalmanovitch model (Urbain, 1987; Kalmanovitch, 1988) was employed which covers a wider range of viscosity values. The reason for choosing this model over Browning model for F-FA LWA was the high estimated viscosity values for F-FA LWA, which was well above 1000 Pa•s where Browning model yield high errors. The following describes the equations for calculating the viscosity of liquid phase using Browning and Urbain-Kalmanovitch models.

The Browning model assumes that the molten slag is a Newtonian fluid (Nicholls and Reid, 1940; Song et al., 2013; Song et al., 2010) and correlates viscosity with temperature (T) using a temperature shift (T_s) (Eqn 1). T_s, as presented in Eqn 2, is a function of a composition parameter A. A is defined as the weighted molar ratio of network former (numerator of Eqn 3) elements to network modifier (denominator of Eqn 3) elements as presented in Eqn 3. The quantity of each component in Eqn 3 is expressed in mole fraction and their summation must add up to unity as shown in Eqn 4.

$$log_{10}\left(\frac{\eta_L}{T-T_s}\right)=\frac{14788}{T-T_S}-10.931 \tag{1}$$

$$T_s = 306.63.ln(A) - 574.31 \tag{2}$$

$$A=\frac{3.19Si^{4+}+0.855Al^{3+}+1.6K^{+}}{0.93Ca^{2+}+1.50Fe^{n+}+1.21Mg^{2+}+0.69Na^{+}+1.35Mn^{n+}+1.47Ti^{4+}+1.91S^{2-}} \tag{3}$$

$$Si^{4+}+Al^{3+}+Ca^{2+}+Fe^{n+}+Mg^{2+}+Na^{+}+K^{+}+Mn^{n+}+Ti^{4+}+S^{2-}=1 \tag{4}$$

Kalmanovitch model was an improvement to Urbain model, which is based on a Weymann type equation. In this model viscosity (η) is related to temperature (T) through constants i.e., a and b, which are dependent on composition of slag. The value of a is a function of b based on Eqn 6. The constant b is a function of Silica (N) and calculated according to Eqs. (7)–(11), where β is calculated based Eqn 12.

$$\eta = aTe^{\frac{1000b}{T}} \tag{5}$$

$$Ln(a) = -0.2812b - 11.8279 \tag{6}$$

$$b = b_0 + b_1N + b_2N^2 + b_3N^3 \tag{7}$$

$$b_0 = 13.8 + 39.9355\beta - 44.049\beta^2 \tag{8}$$

$$b_1 = 30.481 - 117.1505\beta + 129.9978\beta^2 \tag{9}$$

$$b_2 = -40.9429 + 234.0486\beta - 300.04\beta^2 \tag{10}$$

$$b_3 = 60.7619 - 153.9276\beta + 211.1616\beta^2 \tag{11}$$

$$\beta = \frac{CaO+MgO+Na_2O+K_2O+FeO+TiO_2}{Al_2O_3+CaO+MgO+Na_2O+K_2O+FeO+TiO_2} \tag{12}$$

The composition of the liquid phase (slag) (presented in the Appendix) at different temperatures for each LWA was obtained using the thermodynamics modeling software, with varying fluxing agent concentrations, and Eqs. (1)–(12) were used to estimate the viscosity of the liquid phase. Note that the LWA system is composed of a mixture of liquid and solid phases; therefore, the suspension's composite viscosity becomes highly dependent on the volume fraction of solid phase. Thus, to estimate the viscosity of the liquid-solid suspension, the (Krieger and Dougherty, 1959) was used (Eqn 13).:

$$\eta_s = \eta_L\left(1-\frac{\varphi}{\varphi_m}\right)^{-[\eta]\varphi_m} \tag{13}$$

where η_s is the viscosity of the liquid-solid suspension, η_L is the liquid phase (slag) viscosity, φ is the volume fraction of solids (assumed to be equal to the mass fraction, i.e., equal density for solid and liquid phase (Balapour et al., 2021)), ϕ_m is the maximum particle packing fraction, and [η] is the intrinsic viscosity. This equation is applicable in the range 0<ϕ<ϕ_m. In this study, it was assumed that the solid phase particles are spherical, leading to [η] = 2.5, and ϕ_m was calculated according to the model of (Stovall et al., 1986) and was estimated to be 0.74.

4.2. Experimental investigation

4.2.1. Thermal analysis

Thermogravimetric analysis (TGA)and differential thermogravimetric analysis (DTGA) (DTGA curves are the first derivative of TGA curves)were performed to (i) measure the unburnt carbon content of FA, which can directly affect the gas release potential of LWA close to the sintering temperature, and (ii) evaluate the gas release during sintering that forms the LWA pore structure. To measure the unburnt carbon content of raw FA, a 2 atmosphere TGA (2A-TGA) was performed under air and nitrogen. The 2A-TGA was defined as follows: (1) the temperature was held at 100 °C for 5 min; (2) with a 20 °C/min incremental ramp, under nitrogen atmosphere, the temperature was increased to 750 °C; (3) still under nitrogen atmosphere, the temperature was decreased to 100 °C with a 20 °C/min ramp; (4) the atmosphere was switched to air and the temperature was kept at 100 °C for another 5 min; and (5) finally, the temperature was increased to 1000 °C with a 20 °C/min ramp in air. Gas purge flow in all the steps was constant at 25 ml/min. An approximate sample mass of 30 mg of raw FA was used for testing.

To simulate the sintering process and monitor the weight change (corresponding to gas release) of LWA, TGA was performed on the geopolymerized (i.e., underwent the chemical reaction between the dissolved species of aluminates and silicates in a highly alkaline environment to form a three-dimensional aluminosilicate network) (Balapour et al., 2021; Part et al., 2015) pellets under an air atmosphere, where the temperature was increased to 1160 °C from 100 °C with a

[1] Certain commercial equipment, software and/or materials are identified in this paper in order to adequately specify the experimental procedure. In no case does such identification imply recommendation or endorsement by the National Institute of Standards and Technology, nor does it imply that the equipment and/or materials used are necessarily the best available for the purpose.

ramp of 10 °C /min and was held at 1160 °C for 4 min. To prepare the sample for this test, after 24 h of curing the fresh pellet was crushed using a mortar and pestle and then was sieved through a 75 μm size sieve. Approximately 30 mg of collected powder was placed in a crucible pan. Fine refractory ceramic was used between collected powder and TGA pan to prevent molten material, which is formed close to the sintering temperature, adhering to the pan.

4.2.2. X-ray computed tomography (X-CT)

A Zeiss Versa XRM 500 [1] was used to perform X-CT and evaluate the pore structure of produced LWA. The X-ray tube was set for a voltage of 120 kV and a current of 83 μA while the voxel size was set at approximately 19 μm. The exposure time per 2D projection image was approximately 0.45 s, and over 1600 projections were captured throughout a rotation of 360 ° The projections of the LWA were collected using the software supplied with the instrument, and tomographic reconstruction was performed to obtain approximately 1000 2D cross-sectional slices of the LWA, where each slice was about 1000 pixels × 1000 pixels. The visualization and calculations presented in this paper were performed using Dragonfly Software v 2020.1[1] (AASHTO M 295 2018).

4.2.3. Scanning electron microscopy (SEM)

SEM was performed on FA-LWA with 0% and 2% NaOH to further evaluate its pore structure at a micro-scale smaller than resolvable in X-CT. Samples were placed in a container and under vacuum for about 20 min. After that, the vacuum was broken, and low viscosity epoxy was added to the container to cover the whole LWA specimen. The samples were kept under vacuum for another 30 min. Next, samples were kept at room temperature for about 24 h for the epoxy to cure. The samples were sectioned at their mid-plane (x-y plane) using a diamond saw. The polishing and SEM preparation procedure was: wet polishing on SiC paper (i) grit 400 (22 μm) for 2 min under approximately 22 N force (ii) grit 600 (15 μm) for 13 min under approximately 18 N force (iii) grit 800 (10 μm) for 20 min under approximately 9 N force, (iv) and finally polishing on grit 1200 (5 μm) for 30 min under approximately 4 N force. The polished samples were sputter coated with platinum resulting in a coating layer thickness of ~10 nm for SEM observations.

5. Results

5.1. Phase equilibria predictions and quantification of liquid phase content

The left column in Figure S1 shows the predicted phase diagrams for the F-FA systems with 0%, 2%, 4%, 6%, 8%, and 10% NaOH as a function of temperature. In the F-FA+NaOH system, increasing the NaOH concentration transformed mullite and cordierite into feldspar. The feldspar phase was composed of anorthite ($CaAl_2Si_2O_8$), albite ($NaAlSi_3O_8$), and k-feldspar ($KAlSi_3O_8$), which at lower temperature was mainly composed of albite. As the temperature increased the model showed that the main composition transformed toward pure anorthite. This is because albite and k-feldspar have melting points of ≈ 1100 °C and ≈ 1200 °C, respectively, while anorthite's melting temperature is near 1555 °C. While increasing the NaOH concentration to 6% promoted the transformation of mullite and cordierite into feldspar, this did not promote the formation of the liquid phase. At 8% and 10% NaOH concentration, however, the feldspar stability shifted toward formation of nepheline, and increasing the temperature led to the formation of a higher quantity of liquid phase.

The right column in Figure S1 demonstrates the predicted phase diagrams for the C-FA system with 0%, 2%, 4%, 6%, 8%, and 10% of NaOH, as the temperature changed from 800 °C to 1400 °C. The initial melting temperature for all of the NaOH concentrations was predicted to be at approximately 1000 °C. The slightly higher initial melting point for C-FA LWA compared to F-FA LWA is related to the fact that in the Na_2O-Al_2O_3-SiO_2 system, addition of CaO can increase the initial melting temperature (Pacheco-Torgal et al., 2014). Incorporation of a higher NaOH percentage influences the stability of feldspar (mainly composed of anorthite ($CaAl_2Si_2O_8$)), which is mainly a calcium bearing phase toward formation of Nepheline ($NaAlSiO_4$). Feldspar (anorthite) has a melting point of about 1555 °C while the melting point for Nepheline lies between 1100 °C to 1256 °C (Pacheco-Torgal et al., 2014). Therefore, increasing the NaOH content can lower the melting point of the C-FA+flux and promote forming of a higher amount of slag phase.

Fig. 2 shows the liquid phase content at 1160 °C for F-FA and C-FA as a function of NaOH concentration. For F-FA, the liquid phase content with NaOH concentrations of 0% to 6% was in the range of 35% to 40%, while with 8% and 10% NaOH concentration, the liquid phase content increased to 50% and 61%, respectively. On the other hand, for C-FA the liquid phase content gradually increased with incorporation of higher NaOH concentration. The difference between two ashes is directly related to the higher CaO content in C-FA. Higher CaO content in C-FA LWA accompanied by NaOH Addition (i.e., NaOH ≥ 2%) led to formation of higher liquid phase content in the C-FA LWA.

5.2. Viscosity predictions of the LWA liquid-solid system

Fig. 3(a) shows the viscosity of the LWA liquid-solid suspension for F-FA. As can be seen in Fig. 3(a), increasing the NaOH concentration caused the viscosity of the liquid-solid composite to decrease. Although F-FA with 0% NaOH to 6% NaOH exhibited a similar liquid phase content (between 35% to 40%, see Fig. 2), increasing the NaOH concentration led to a higher molar fraction of Na^+, which has a fluxing role, in the liquid phase composition and so reduced the liquid phase viscosity and consequently the total composite viscosity. Among F-FA LWA the lowest observed viscosity was that of F-FA 10% (picture shown in Fig. 3(a)) which was equal to 1175 Pa•s. (Balapour et al., 2021) found that maintaining a viscosity value higher than 100 Pa•s for the bottom ash LWA will preserve its spherical shape under gravitational forces, which was also confirmed in the case of F-FA LWA in this study.

Fig. 3(b) shows the LWA liquid-solid suspension viscosity for the C-FA system. Incorporating higher concentrations of NaOH gradually reduced composite viscosity by (i) promoting the formation of a higher liquid phase content and (ii) intensifying the amount of Na^+ in the liquid phase. Na^+ with a fluxing role (see Eqn 3) acts as a network breaker and therefore reduced the viscosity of the liquid phase. Generally, the lower viscosity values for C-FA in comparison with F-FA were due to the fact that C-FA had a higher content of CaO (see Table 1) leading to higher molar fraction of Ca^{2+} in the composite. Ca^{2+} has a notable fluxing role (see Eqn 3) and can substantially reduce the viscosity of the liquid phase. C-FA 10% LW, which had the lowest viscosity value is shown in Fig. 3

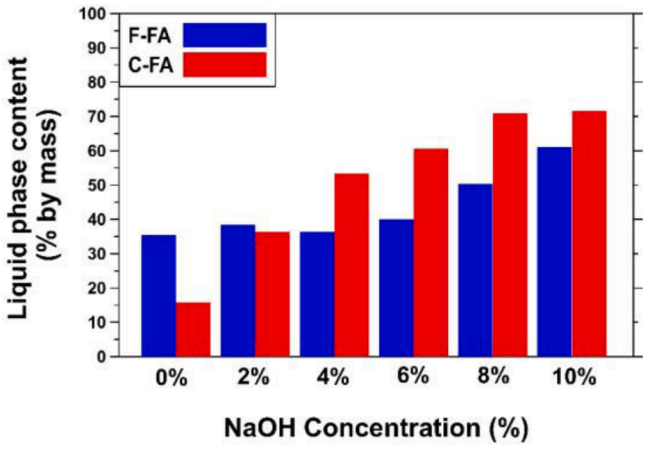

Fig. 2. Liquid phase (i.e., slag) content of F-FA and C-FA at 1160 °C as a function of NaOH concentration.

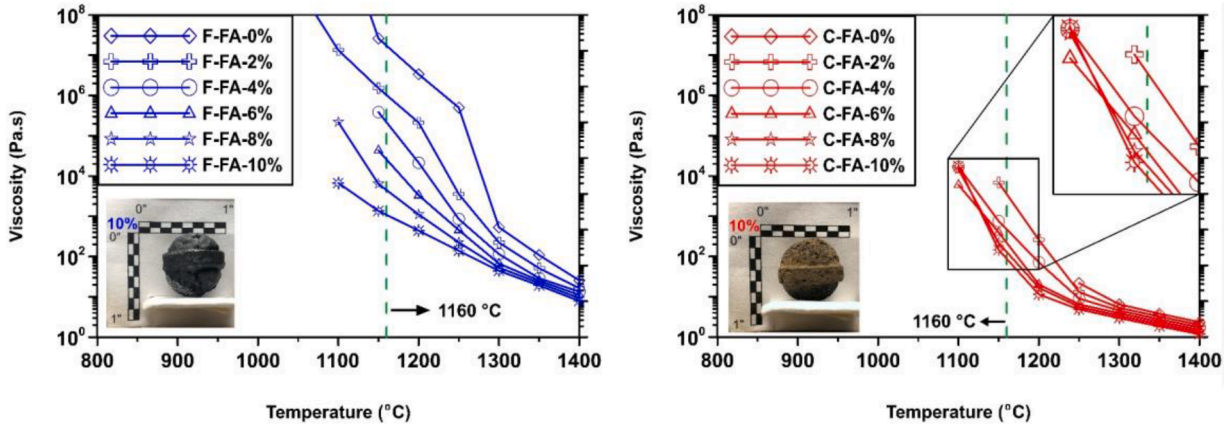

Fig. 3. Viscosity of LWA liquid-solid suspension with various NaOH concentrations, estimated using combination of Urbain- Kalmanovitch and Krieger-Dougherty models for (a) F-FA LWA and Browning and Krieger-Dougherty models for (b) C-FA . The picture of F-FA 10% and C-FA 10% are shown in figure (a) and (b) respectively. The dashed green lines show the furnace's operating temperature. (Note: for F-FA LWA some data points are placed out of the y-axis maximum viscosity and are not shown).

(b). As can be seen the spherical shape of this LWA was preserved after sintering. The associated calculated viscosity for this LWA was 119 Pa•s, which was higher than 100 Pa•s, confirming the previous finding (Balapour et al., 2021) of the authors that a viscosity value greater than 100 Pa•s can maintain the spherical shape for the LWA under gravitational forces during sintering.

5.3. Gas release potential during sintering

5.3.1. Unburnt carbon content determination

Previously, it was shown that the unburnt carbon content available in the system can influence the extent of gas release close to the sintering temperature (Dondi et al., 2016; Paya et al., 1998); therefore, it is important to determine the unburnt carbon content of the two fly ash samples. Figure S2 and Figure S3 show the 2A-TGA performed on F-FA and C-FA respectively. For F-FA, as shown in Figure S2 (a) under nitrogen atmosphere, the weight loss up to about 500 °C could be related to evaporation of moisture as a very gradual weight reduction occurs (~ 1% mass reduction). On the other hand, the steep weight reduction from about 500 °C to about 750 °C could be attributed to the decomposition of amorphous phases in the ash (see Table 2). In the second step, as shown in Figure S2 (b) at air atmosphere, the weight loss was likely due to oxidation of unburnt carbon (Paya et al., 1998; Mohebbi et al., 2015). The decomposition in the second step started at about 600 °C, which shows an overlap with the decomposition of amorphous phases (see Table 2) in the first step i.e., under nitrogen gas; therefore, it indicates that the amorphous phases and carbon oxidation overlap in the temperature range for their decomposition. In the case of C-FA in Figure S3 (a), similar to F-FA, the weight loss before about 500 °C could be related to gradual evaporation of water (~ 1% mass reduction), while after this temperature the decomposition can be related to amorphous phase. Similarly, the weight loss under air atmosphere demonstrated in Figure S3 (b), which started at about 500 °C was related to oxidation of unburnt carbon (Paya et al., 1998). The unburnt carbon content for F-FA and C-FA was determined to be 2.3% and 7.0% by mass, respectively.

5.3.2. Gas release determination of geopolymerized pellets using TGA

TGA was performed on geopolymerized pellets to simulate the sintering process and evaluate the gas release potential of LWA that leads to the bloating mechanism. Figure S4 (a1) to (a6) shows the TGA/DTG curves for the F-FA with incremental concentration of NaOH from 0% to 10%, respectively. As the temperature increased from room temperature to 1160 °C, mass loss peaks were observed that corresponded to phase decomposition and subsequent gas release. The peak labelled H is related to the release of free and bound water from the structure of the material (Scrivener et al., 2018) . As the NaOH concentration increased, a peak indicated as Am_1 intensified in the range 400 °C to 650 °C, which corresponded to the decomposition of N-A-S-H gel in the material (Park et al., 2016). The peak labelled C occurring at 650 °C was likely related to carbon oxidation (Paya et al., 1998; Mohebbi et al., 2015). However, as was shown in Sec 0, the temperature range for the decomposition of amorphous phases and carbon oxidation overlap with each other. From the 2A-TGA test, the carbon oxidation occurred between 600 °C and 900 °C, with a peak at about 800 °C. However, in the case of geopolymerized pellets, it appears that carbon oxidation peaked at ~ 650 °C. Two more decompositions occurred at temperatures greater than 950 °C, which were merged at the 0% NaOH concentration and started to separate as the NaOH concentration increased. These two decompositions were seemingly related to anhydrite (labelled with A) and hematite (labelled with $\overline{H}$) (Salman and Khraishi, 1988; Lee et al., 2019). It has been previously shown that hematite reduction to release carbon dioxide could be facilitated by the presence of unburnt carbon in the ash (Balapour et al., 2021; Paya et al., 1998; Wie et al., 2020). Therefore, it is speculated that the observed gas release is partly related to reduction of hematite by the unburnt carbon.

Figure S4 (b1) to (b6) shows the TGA performed on C-FA with the NaOH concentration varying from 0% to 10%. The H peak, occurring at a constant temperature of about 100 °C, was related to free and bound moisture release (Scrivener et al., 2018). The sharp peak designated by $C+Am_1$ was related to co-occurrence of amorphous phase decomposition and oxidation of free carbon from the material occurring at the range of 500 °C to 700 °C (Paya et al., 1998). By increasing the NaOH concentration from 0% to 10%, a peak located at the shoulder of the $C+Am_1$ peak appeared, designated by Am_2, which most probably was related to the decomposition of amorphous C-(N)-A-S-H gel (Pacheco--Torgal et al., 2014). Finally, two peaks were again identifiable in the range of 950 °C to 1160 °C, which corresponded to anhydrite decomposition (peak A) and carbon dioxide release from hematite (peak $\overline{H}$) (Salman and Khraishi, 1988; Lee et al., 2019). Comparing C-FA with F-FA TGA results, C-FA releases gaseous phase content almost at three times the rate of F-FA near sintering temperature (i.e., from onset of liquid phase formation to about 1160 °C). This could be related to the fact that C-FA had 3% and 7% anhydrite and unburnt carbon, respectively, while F-FA had 1.86% and 2.3% (see Table 1 and Table 2). Greater unburnt carbon could be a potential source to facilitate reduction of hematite (Balapour et al., 2021; Paya et al., 1998; Wie et al., 2020).

5.4. Evaluation of LWA pore structure using X-CT

Figure S5 shows a 2D slice of F-FA (left column) and C-FA (right column) with incremental NaOH concentration. For F-FA LWA, a "core-shell" morphology could be identified in this LWA. These two regions are separated by the circular/elliptical white dashed line on the 2D slices. The "shell" refers to the outer part of white dashed circle/ellipse, where spherical type pores were located (Ducman et al., 2013). While the pores formed in the shell of F-FA-0% were of size about 100 μm, the general trend implied that upon incremental NaOH addition, the pores located in the LWA shell became larger. On the other hand, in the middle part of the LWA (inner part of the white dashed line circle/ellipse, defined as "core"), surrounded by the shell, the pores are more interconnected and elongated. One potential reason for the formation of this morphology is related to the heat barrier created by the shell, which delays the heat transfer to the middle part of the LWA (Billen et al., 2018). This phenomenon probably resulted in the observation that the shell of LWA tend to have a higher gray scale value (GSV) compared to the core, which corresponds to higher density (Brisard et al., 2020; Hanna and Ketcham, 2017). This observation is more pronounced in the case of C-FA LWA. Interestingly, some major cracks were observed in the core of F-FA-4% LWA, and to a lesser extent for F-FA-8% and F-FA-10%. Two possible reasons could be: (i) occurrence of thermal cracking due to shrinkage during rapid sintering and (ii) displacement of the core of LWA by the released gas causing internal pressure and finally cracking (Wie and Lee, 2020).

For C-FA-0%, extensive cracking occurred, which could possibly be related to the two explanations given for F-FA. Upon adding NaOH to the LWA, the core-shell morphology also occurred for the C-FA LWA. The shell contains embedded spherical-type pores, which indicated the fluxing role of NaOH and formation of the liquid phase in the LWA. Higher than 6% NaOH, the shell's thickness increased noticeably and the LWA core became smaller. It is speculated that the formation of liquid phase, promoted by higher NaOH percentage, leads to integrity and higher strength for the LWA (Balapour et al., 2021), which is where the formation of cracks could be suppressed. However, as can be seen in Figure S5, for C-FA 2%, even in the presence of NaOH, some cracks were formed in the core of the LWA. The cracks in the LWA core caused formation of an island-type solid phase, as indicated by the white dashed line. Note that phase connectivity in 3D is different than in 2D. Since the LWA held together outside of the mold, the solid core phase must interconnected, rather than isolated fragments. The presence of the cracks in the core regions could potentially affect the structural integrity of the LWA. On the other hand, it is plausible that cracks could help with moisture transport and dynamics in the LWA pores. As it mentioned before, the shell appears to have higher GSV and density, which is likely related to the shell acting as an insulating layer that delays heat transfer to the core of LWA. Therefore, the shell experienced higher temperature compared to the core and more densification has occurred in the shell (Billen et al., 2018; Lee et al., 2019; Ducman et al., 2013).

6. Discussion

This section contains discussion of the three required parameters for successful production of LWA through sintering: (i) sufficient amount of liquid phase, (ii) appropriate viscosity for the liquid-solid suspension, and (iii) adequate amount of effective gas release. The effects of these parameters on the final LWA morphology and an operable working zone for the production of LWA are discussed.

6.1. Formation of liquid phase during sintering

The formation of sufficient amount of liquid phase in the LWA is a crucial factor to provide a medium for pore expansion and consequently the bloating mechanism, as well as providing sufficient bonding between partially molten FA particles during sintering (Dondi et al., 2016; Balapour et al., 2020). In our previous study (Balapour et al., 2021), it was found that the presence of a minimum mass fraction of 50% liquid phase in the LWA made from **bottom ash** (with a random shape particle size ranging from 600 μm to 75 μm) could assure that the bloating mechanism was achieved. However, in this study, the raw material is **fly ash (FA)**, which has a considerably smaller particle size distribution (average particle size of ~ 20 μm with spherical shape (Chindaprasirt et al., 2009)) and correspondingly higher surface area compared with bottom ash. It is expected that a smaller particle size distribution (higher surface area) can promote formation of higher liquid phase content (German et al., 2009), which cannot be captured by thermodynamic modeling (German, 2013). Therefore, a smaller limit for the liquid phase content may be required to ensure pore expansion in the LWA.

First, we correlated the liquid phase content to the X-CT observations. Starting with F-FA 0% LWA, which had 35.4% by mass liquid phase content, the small spherical type pores (in the 100 μm size range) were formed in the LWA shell. As the NaOH concentration gradually increased, the liquid phase content increased accordingly and the X-CT observations showed the formation of larger spherical/round type pores (in the 500 μm size range) in the LWA shell. All the F-FA LWA had a liquid phase content of greater than 35%.

In the case of C-FA LWA, the liquid phase content for C-FA 0% was 15.7%. Correlating that with X-CT observations (see Figure S5) of C-FA 0%, no spherical-type pores were observed in the LWA shell, which implies that liquid phase content was not enough to lead to formation of gas-filled pores and active a bloating mechanism. For C-FA with NaOH $\geq$ 2%, the liquid phase content passed 35% and accordingly round pores started to form in the shell of LWA. In addition, as the NaOH concentration gradually increased the fluxing role of NaOH helped with formation of more liquid phase content (see Fig. 2), which provided a greater medium for pore expansion in the LWA. One of the reasons that C-FA LWA formed bigger pores compared with F-FA LWA is the higher liquid phase content for the former at each NaOH concentration (except 0%) (see Fig. 2). Correlation between the liquid phase content and X-CT observations for both types of FA-LWA suggested that 35% is the minimum liquid content allowing the formation of pores in the LWA shell region for both kinds of FA.

6.2. Viscosity of liquid-solid phase during sintering

The viscosity of the liquid phase plays two major roles in the successful production of LWA through sintering: (i) the value of the viscosity must be such that it enables the pores created by the emission of the gaseous phase into the liquid phase to expand and contribute to the bloating of LWA (the smaller the viscosity the easier pore expansion occurs), and (ii) the value of the viscosity must be such that it prevents excessive deformation for the LWA under gravitational force or the force created by pore expansion before solidification occurs in order to maintain a spherical LWA shape. For F-FA LWA, as shown in Fig. 3, increasing the NaOH concentration decreased the viscosity of liquid-solid phase. Correlating this behavior with that of the X-CT images, it was observed that by increasing the NaOH concentration the pores became larger; also, some pore joining occurred. This is likely due to the decreasing viscosity of the liquid-solid phase, which allowed easier expansion and movement of pores in the liquid phase. Similar trends were also observed for C-FA LWA, i.e., as the NaOH concentration increased, the viscosity of the liquid-solid phase decreased, which allowed for easier expansion and pore-joining. A comparison between the pore structure of C-FA LWA and F-FA LWA implies formation of larger pores in the former. One of the reasons related to this difference is the smaller viscosity for the liquid-solid phase in C-FA LWA compared to F-FA LWA (see Fig. 3). C-FA possessed a higher content of CaO, which has a notable fluxing role and thus reduces the viscosity considerably.

6.3. Gaseous phase formation during sintering

Formation of a gaseous phase close to the sintering temperature, which can then be captured by the liquid phase, ensures pore creation and consequently bloating in the LWA. In this study, the effective gas release ($g_{effective}$ expressed in% by mass) that can contribute to bloating was defined as the amount of released gas between the initial melting temperature (obtained from the phase diagrams in Figure S1) and ultimate sintering temperature i.e., 1160 °C. Fig. 4 shows $g_{effective}$ for F-FA and C-FA at different NaOH concentrations based on the TGA results. The data indicated $g_{effective}$ amount varied from 0.64% to 3.68% considering both materials. (Balapour et al., 2021) showed that when sufficient liquid phase forms, with the liquid-solid viscosity in an appropriate range, even $g_{effective} = 0.24\%$ ensured formation of gas filled pores in the LWA made from bottom ash. In this study, the minimum $g_{effective}$ measured using TGA was 0.64%, corresponding to F-FA 6%. The XCT 2D slice for F-FA 6% confirmed the formation of spherical-type pores. Therefore, another possible reason for larger pores formed in C-FA LWA compared with F-FA LWA could be related to the higher values of $g_{effective}$ by C-FA LWA (see Fig. 4).

Based on Fig. 4, TGA results indicated a similar trend for the value of $g_{effective}$, where a slight reduction was observed for both FAs as the NaOH concentration increased. The thermodynamic modeling done in Section 0 indicated that at low NaOH concentration the gas release was a mixture of O_2, SO_2, and SO_3. However, as the NaOH concentration increased the O_2 portion of the gas mixture decreased. This could be related to oxidation reactions occurring at high temperature, resulting in oxygen absorption. Higher values of $g_{effective}$ for C-FA in comparison with F-FA was related to both larger amounts of SO_2+SO_3 and O_2 gaseous phases released by this material. This could be partly explained by a higher SO_3 content in the chemical composition of C-FA (see Table 1). It should be noted that since the unburnt carbon is not considered in thermodynamics modeling the gas release predictions are O_2. It is expected that including carbon in thermodynamics modeling will change gaseous products to CO_2.

6.4. Pore structure evaluation of LWA with 0% NaOH and 2% NaOH

SEM images for F-FA 0%, F-FA 2%, C-FA 0%, and C-FA 2% are shown in Fig. 5. As can be seen for F-FA 0% and F-FA 2%, prevalent formation of spherical/round type pores in the liquid phase can be confirmed. Correlating this observation with the liquid phase content predictions indicated that since these two LWA had a liquid phase greater than 35% spherical type pores (an indication of bloating mechanism) were successfully formed. In contrast, the SEM image of C-FA 0% showed minimal formation of spherical pores in the LWA, which implies that liquid phase content was not sufficient for occurrence of bloating. The liquid phase content for this LWA was 15.7%. In addition, due to insufficient melting, a great degree of bonding gap among fly ash particles was observed, which could lead to diminished mechanical strength for the LWA. On the other hand, for C-FA 2%, where the predicted liquid phase content was 36.4%, there was a large amount of spherical pore formation in the liquid phase.

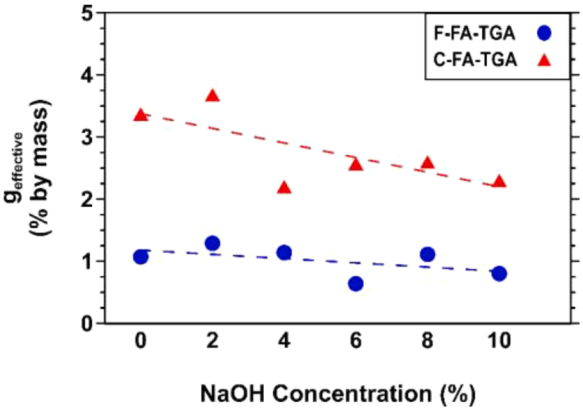

Fig. 4. The effective gas release during sintering measured using TGA for F-FA and C-FA LWA with varying NaOH concentration.

6.5. Required technical conditions for successful LWA production

To put the three required conditions (liquid phase content, viscosity of liquid-solid phase, and effective gas release amount) into perspective, a diagram was developed based on these quantified conditions, Fig. 6. The location of each circle, associated with the produced LWA, is based on its liquid phase content and viscosity, and the color is associated with the $g_{effective}$ value for that LWA obtained from TGA results. C-FA 0% LWA is not placed on the diagram since the viscosity was not calculable for the LWA owing to small liquid phase content. As was previously indicated, a minimum 35% liquid phase content was necessary to provide a medium for pore expansion. The red dashed line shows the limit associated with the liquid phase content. (Balapour et al., 2021) found that for the LWA produced from bottom ash a minimum 100 Pa•S viscosity was required to prevent deformation under gravitational force and retain the spherical shape, which was also found in this study. Correlating the XCT and SEM images with viscosity values, it was found that distinguishable pore expansion started to occur in F-FA 0% LWA. F-FA-0% had a viscosity of $2.2–10^7$ Pa•s. This observation along with limitations inherent to viscosity models (such as estimation of viscosity at a temperature lower than critical viscosity i.e., the temperature which the viscosity of liquid phase sharply changes with temperature (Vargas et al., 2001; Luan et al., 2014)) prevents one from suggesting an upper bound for viscosity value at this point. Based on the proposed limitations, F-FA 0%, F-FA 2%, F-FA 4%, F-FA 6%, F-FA 8%, F-FA 10%, C-FA 2%, C-FA 4%, C-FA 6%, C-FA 8%, and C-FA 10% were placed in this working zone. In this working zone, the minimum $g_{effective}$ was that of F-FA 6%, which was 0.64%. Based on this work and previous work (Balapour et al., 2021), it appears that even a minimum value of 0.24% for $g_{effective}$ could create adequate LWA pore creation when liquid phase and viscosity conditions are satisfied.

7. Conclusions

This paper quantitatively investigated the three necessary conditions for the production of LWA from low and high calcium waste coal combustion FA through a sintering process. These three required conditions are: (i) formation of an adequate liquid phase content, (ii) appropriate viscosity for the liquid-solid phase, and (iii) release of sufficient amount of gaseous phase for adequate pore formation. The following primary conclusions can be drawn from this study:

(i) Formation of at least 35% liquid phase content was necessary for both types of FA to ensure gas-filled pore creation in the LWA. For the LWA with liquid phase content less than this limitation, gas filled pores rarely could be observed.

(ii) It was found that the viscosity of the liquid-solid phase controls the pore size in the LWA pore structure. Larger pores were observed in C-FA LWA, likely because of its lower viscosity, compared with F-FA LWA, which had higher viscosity. A lower bound of 100 Pa•s was confirmed to prevent the deformation of LWA during sintering by gravitational forces to keep the spherical shape of LWA. The highest predicated viscosity was $2.2 \cdot 10^7$ Pa•s for F-FA-0%, where SEM observation showed formation spherical pores that indicate successful occurrence of the bloating mechanism.

(iii) The value of $g_{effective}$ was found to be necessary for pore creation in the LWA considering that the requirements mentioned in (i) and (ii) were satisfied. The measured $g_{effective}$ for F-FA ranged

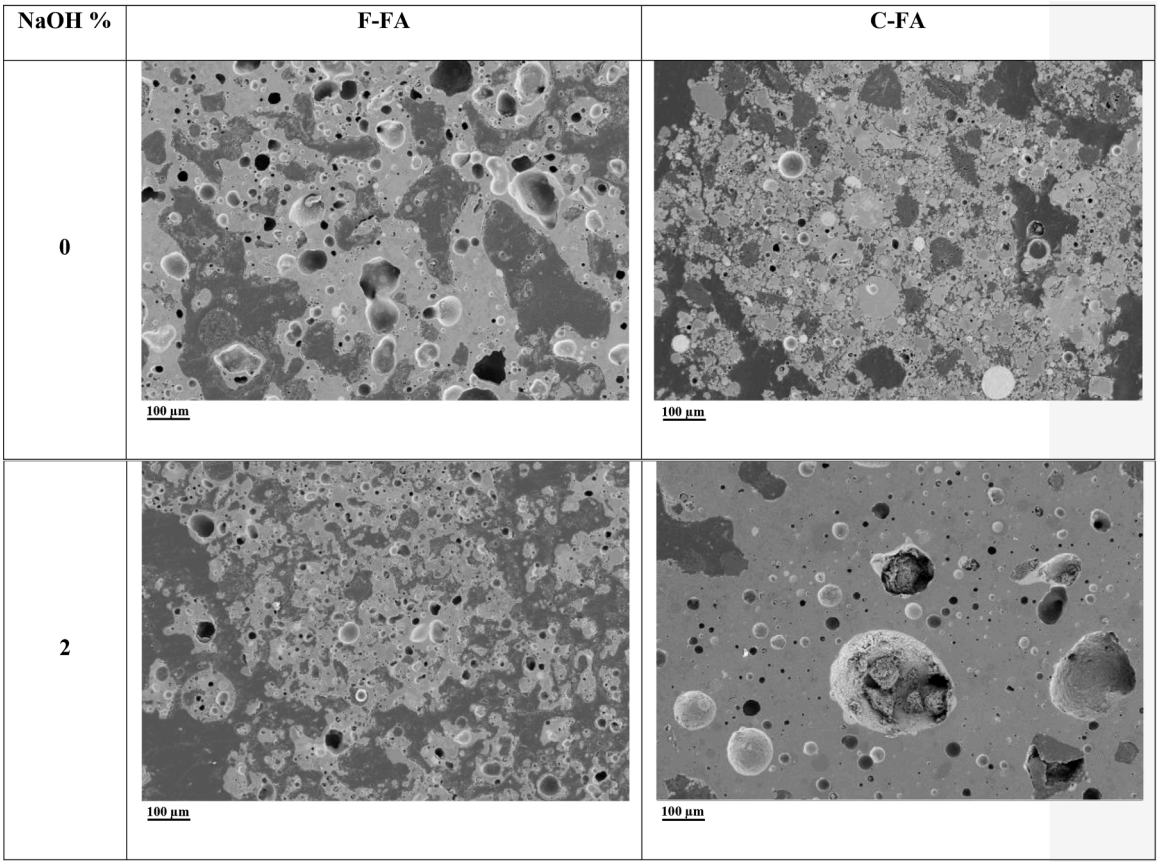

Fig. 5. SEM micrographs for F-FA 0%, F-FA 2%, C-FA0%, and C-FA 2%. Images were all taken at 10 kV, 100X magnification.

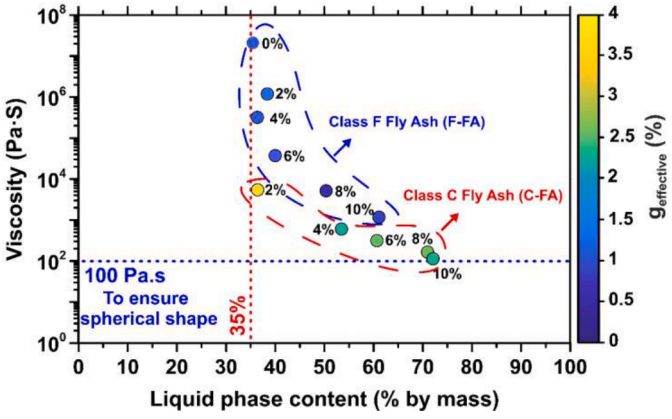

Fig. 6. Holistic view of LWA regarding the three necessary conditions for LWA production.

from 0.64% to 1.29%, while this value for C-FA ranged from 2.2% to 3.68%. On average, C-FA LWA had 2.75 times greater $g_{effective}$ compared to F-FA LWA. The higher $g_{effective}$ could be one possible reason for the formation of larger pores in C-FA LWA. The gas release was related to the presence of hematite and anhydrite in the raw FA. In addition, it was found that presence of higher unburnt carbon content and anhydrite in C-FA could be the reason for higher $g_{effective}$ of LWA prepared with this material.

Based on the predictive diagram developed in this study, it was found that even without addition of NaOH, a successfully bloated LWA could be produced from F-FA. However, for C-FA LWA an addition of at least 2% NaOH was needed for successful LWA production. Only using these minimum concentrations could be beneficial from a cost and environmental impact point of view. However, at the same time, the functionality (i.e., engineering properties such as specific gravity, compressive strength, water absorption, and water desorption) of these LWA needs to be assessed to determine the NaOH concentrations that are also optimal for the LWA properties. This is because different NaOH concentrations could significantly influence the engineering performance of LWA (Balapour et al., 2020).

FA-LWA could be used for different applications such as lightweight concrete production, internal curing of concrete, green roofs, and embankment, where each application may require specific and different LWA engineering properties. Therefore, future work will involve two main areas: (i) assessing the engineering properties of these FA LWA, which include specific gravity, moisture (water) dynamics in the pore structure, pore size distribution, and compressive strength, and (ii) scaling up the production of spherical FA-LWA using a pelletizer (to produce spherical fresh pellets) and rotary furnace to bring the process closer to pilot-scale production to address the underutilization of landfilled waste FA.

Adoption of the proposed technology at large scale can address the negative environmental impacts associated with landfilled waste CCPs by converting this material to value-added LWA. Two prominent instances of the negative environmental impacts of landfilled waste CCPs are the catastrophic Kingston Fossil Plant coal fly ash slurry spill (Tennessee, 2008) (BOURNE, 2019) and Dan River coal ash spill (North Carolina, 2014) (Hitt et al., 2019), where long-term environmental

damage was caused, and human health was compromised. The cost associated with cleaning the Kingston fly ash slurry spill was estimated to be $1.1 billion (AASHTO M 295 2017). Moreover, the waste CCPs landfills require annual budget allocation for construction and maintenance burdened which further impose on financial and administrative burdens on coal powerplants. Therefore, adopting the technology introduced in this paper not only can divert waste CCPs from landfills, but can promote the local production of LWA for construction industry to address the supply chain issues associated with this material in the US.

CRediT authorship contribution statement

Mohammad Balapour: Data curation, Conceptualization, Investigation, Formal analysis, Validation, Visualization, Writing – original draft, Writing – review & editing. **Thiha Thway:** Investigation. **Rathin Rao:** Investigation. **Newell Moser:** Investigation, Writing – review & editing. **Edward J. Garboczi:** Investigation, Writing – review & editing. **Y Grace Hsuan:** Conceptualization, Writing – review & editing. **Yaghoob Farnam:** Funding acquisition, Conceptualization, Supervision, Writing – review & editing.

Declaration of Competing Interest

The authors declare that they have no known competing financial interests or personal relationships that could have appeared to influence the work reported in this paper.

Acknowledgement

This work was supported in part by the National Science Foundation (NSF CMMI – 1550723 and PFI– TT 1918838) and was performed at Drexel University in the Advanced and Sustainable Infrastructure Materials (ASIM) Lab. Any opinions, findings, and conclusions or recommendations expressed in this material are those of the authors and do not necessarily reflect the views of the National Science Foundation.

Supplementary materials

Supplementary data associated with this article can be found, in the online version, at 10.1016/j.resconrec.2021.106050.

References

Mousa, A., Mahgoub, M., Hussein, M., 2018. Lightweight concrete in America: presence and challenges. Sustain. Prod. Consum. 15, 131–144.
Dondi, M., Cappelletti, P., D'Amore, M., de Gennaro, R., Graziano, S.F., Langella, A., Raimondo, M., Zanelli, C., 2016. Lightweight aggregates from waste materials: reappraisal of expansion behavior and prediction schemes for bloating. Constr. Build. Mater. 127, 394–409. https://doi.org/10.1016/j.conbuildmat.2016.09.111.
Cheeseman, C.R., Makinde, A., Bethanis, S., 2005. Properties of lightweight aggregate produced by rapid sintering of incinerator bottom ash. Resour. Conserv. Recycl. 43, 147–162.
Kourti, I., Cheeseman, C.R., 2010. Properties and microstructure of lightweight aggregate produced from lignite coal fly ash and recycled glass. Resour. Conserv. Recycl. 54, 769–775.
Balapour, M., Zhao, W., Garboczi, E.J., Oo, N.Y., Spatari, S., Hsuan, Y.G., Billen, P., Farnam, Y., 2020. Potential use of lightweight aggregate (LWA) produced from bottom coal ash for internal curing of concrete systems. Cem. Concr. Compos. 105, 103428.
A.C.A. Association, ACAA 2018 CCP survey results, (2018).
Billen, P., Mazzotti, M., Pandelaers, L., Ye oo, N., Zhao, W., Liu, Z., Redus, J., Loya, I. Diaz, Bartoli, I., Farnam, Y., Spatari, S., Hsuan, Y.G., 2018. Melt ceramics from coal ash: constitutive product design using thermal and flow properties. Resour. Conserv. Recycl. 132, 168–177. https://doi.org/10.1016/j.resconrec.2018.01.035.
EPA, 2.0.1.5, 2015. 40 CFR Parts 257 and 261: hazardous and solid waste management system: disposal of coal combustion residues from electric utilities. Fed. Regist. 80, 21302–21501.
Balapour, M., Rao, R., Spatari, S., Hsuan, Y.G., Farnam, Y., May . Engineering Properties of Fly Ash-Based Lightweight Aggregate. In: World Coal Ash Conf. (WOCA), St. Louis, MO.
Wei, Y.-L., Lin, Y.-Y., 2009. Role of Fe compounds in light aggregate formation from a reservoir sediment. J. Hazard. Mater. 171, 111–115.
Wei, Y.-L., Yang, J.-C., Ko, K.-W., 2012. Evidence for a new mechanism of Fe 2 O 3 decomposition in lightweight aggregate formation. Environ. Chem. Lett. 10, 41–47.
Ramamurthy, K., Harikrishnan, K.I., 2006. Influence of binders on properties of sintered fly ash aggregate. Cem. Concr. Compos. 28, 33–38.
Kockal, N.U., Ozturan, T., 2010. Effects of lightweight fly ash aggregate properties on the behavior of lightweight concretes. J. Hazard. Mater. 179, 954–965.
Verbinnen, B., Billen, P., Van Caneghem, J., Vandecasteele, C., 2017. Recycling of MSWI bottom ash: a review of chemical barriers, engineering applications and treatment technologies. Waste Biomass Valorization 8, 1453–1466.
Riley, C.M., 1951. Relation of chemical properties to the bloating of clays. J. Am. Ceram. Soc. 34, 121–128.
Balapour, M., Rao, R., Garboczi, E.J., Spatari, S., Hsuan, Y.G., Billen, P., Farnam, Y., 2021. Thermochemical principles of the production of lightweight aggregates from waste coal bottom ash. J. Am. Ceram. Soc. 104, 613–634.
Aineto, M., Acosta, A., Rincon, J.M., Romero, M., 2006. Thermal expansion of slag and fly ash from coal gasification in IGCC power plant. Fuel 85, 2352–2358.
Balapour, M., 2020. Characterizing Physical Properties of Lightweight Aggregate Made from Waste Coal Ash Using X-Ray Computed Tomography.
ASTM C618-19, 2019. Standard Specification for Coal Fly Ash and Raw or Calcined Natural Pozzolan for Use in Concrete. ASTM Int., West Conshohocken, PA, USA.
AASHTO M 295, 2007. Standard specification for coal fly ash and raw or calcined natural Pozzolan for use in concrete. Am. Assoc. State Highw. Transp. Off.
Browning, G.J., Bryant, G.W., Hurst, H.J., Lucas, J.A., Wall, T.F., 2003. An empirical method for the prediction of coal ash slag viscosity. Energy Fuels 17, 731–737.
Urbain, G., 1987. Viscosity estimation of slags. Steel Res 58, 111–116.
Kalmanovitch, D.P., 1988. An effective model of viscosity for ash deposition phenomena. In: Proc. Eng. Found. Conf. Miner. Matter Ash Depos. from Coal, 1988, pp. 89–101.
Nicholls, P., Reid, W.T., 1940. Viscosity of coal-ash slags. J. Eng. Power;(United States) 62, 141–153.
Song, W., Tang, L., Zhu, Z., Ninomiya, Y., 2013. Rheological evolution and crystallization response of molten coal ash slag at high temperatures. AIChE J. 59, 2726–2742.
Song, W., Tang, L., Zhu, X., Wu, Y., Zhu, Z., Koyama, S., 2010. Flow properties and rheology of slag from coal gasification. Fuel 89, 1709–1715.
Krieger, I.M., Dougherty, T.J., 1959. A mechanism for non-Newtonian flow in suspensions of rigid spheres. Trans. Soc. Rheol. 3, 137–152.
Stovall, T., De Larrard, F., Buil, M., 1986. Linear packing density model of grain mixtures. Powder Technol. 48, 1–12.
Part, W.K., Ramli, M., Cheah, C.B., 2015. An overview on the influence of various factors on the properties of geopolymer concrete derived from industrial by-products. Constr. Build. Mater. 77, 370–395.
Dragonfly, (2018). https://www.theobjects.com/dragonfly/index.html.
Pacheco-Torgal, F., Labrincha, J., Leonelli, C., Palomo, A., Chindaprasit, P., 2014. Handbook of Alkali-Activated cements, Mortars and Concretes. Elsevier.
Paya, J., Monzo, J., Borrachero, M.V., Perris, E., Amahjour, F., 1998. Thermogravimetric methods for determining carbon content in fly ashes. Cem. Concr. Res. 28, 675–686.
Mohebbi, M., Rajabipour, F., Scheetz, B.E., May 2015. Reliability of loss on ignition (LOI) test for determining the unburned carbon content in fly ash. In: World Coal Ash Conf. (WOCA), Nashville, TN, pp. 5–7.
Scrivener, K., Snellings, R., Lothenbach, B., 2018. A Practical Guide to Microstructural Analysis of Cementitious Materials. CRC Press.
Park, S.M., Jang, J.G., Lee, N.K., Lee, H.-K., 2016. Physicochemical properties of binder gel in alkali-activated fly ash/slag exposed to high temperatures. Cem. Concr. Res. 89, 72–79.
Salman, O.A., Khraishi, N., 1988. Thermal decomposition of limestone and gypsum by solar energy. Sol. Energy. 41, 305–308.
Lee, K.H., Lee, J.H., Wie, Y.M., Lee, K.G., 2019. Bloating mechanism of lightweight aggregates due to ramping rate. Adv. Mater. Sci. Eng. 2019 1–12.
Wie, Y.M., Lee, K.G., Lee, K.H., 2020. Chemical design of lightweight aggregate to prevent adhesion at bloating activation temperature. J. Asian Ceram. Soc. 1–10.
Ducman, V., Korat, L., Legat, A., Mirtič, B., 2013. X-ray micro-tomography investigation of the foaming process in the system of waste glass–silica mud–MnO2. Mater. Charact. 86, 316–321.
Brisard, S., Serdar, M., Monteiro, P.J.M., 2020. Multiscale X-ray tomography of cementitious materials: a review. Cem. Concr. Res. 128, 105824.
Hanna, R.D., Ketcham, R.A., 2017. X-ray computed tomography of planetary materials: a primer and review of recent studies. Chemie Der Erde-Geochemistry 77, 547–572.
Wie, Y.M., Lee, K.G., 2020. Composition design of the optimum bloating activation condition for artificial lightweight aggregate using coal ash. J. Korean Ceram. Soc. 57, 220–230.
Chindaprasirt, P., Jaturapitakkul, C., Chalee, W., Rattanasak, U., 2009. Comparative study on the characteristics of fly ash and bottom ash geopolymers. Waste Manag 29, 539–543.
German, R.M., Suri, P., Park, S.J., 2009. Liquid phase sintering. J. Mater. Sci. 44, 1–39.
German, R.M., 2013. Liquid Phase Sintering. Springer Science & Business Media.
Vargas, S., Frandsen, F.J., Dam-Johansen, K., 2001. Rheological properties of high-temperature melts of coal ashes and other silicates. Prog. Energy Combust. Sci. 27, 237–429.

Luan, C., You, C., Zhang, D., 2014. An experimental investigation into the characteristics and deposition mechanism of high-viscosity coal ash. Fuel 119, 14–20.
BOURNE, J.JOEL K., 2019. Coal's other dark side: Toxic ash that can poison water and people. https://www.epa.gov/tn/epa-response-kingston-tva-coal-ash-spill.
Hitt, M.A., Ash, Coal, Water, Clean, 2019. The Dan River Spill Five Years Later. https://www.sierraclub.org/articles/2019/02/coal-ash-and-clean-water-dan-river-spill-five-years-later.
Watts Bar Reservoir has returned to conditions before Kingston coal ash spill, EPA says, Oak Ridge Today, 2017.